Inorganic Chemistry

Article

pubs.acs.org/IC

$(BMI)_3LnCl_6$ Crystals as Models for the Coordination Environment of $LnCl_3$ (Ln = Sm, Eu, Dy, Er, Yb) in 1-Butyl-3-methylimidazolium Chloride Ionic-Liquid Solution

Yulun Han, Cuikun Lin, Qingguo Meng, Fengrong Dai, Andrew G. Sykes, Mary T. Berry, and P. Stanley May*

Department of Chemistry, University of South Dakota, 414 East Clark Street, Vermillion, South Dakota 57069, United States

Supporting Information

ABSTRACT: A series of $(BMI)_3LnCl_6$ (Ln = Sm, Eu, Dy, Er, Yb) crystals was prepared from solutions of $LnCl_3$ dissolved in the ionic liquid, 1-butyl-3-methylimidazolium chloride (BMICl). Crystals with Ln = 5% Sm + 95% Gd and with Ln = 5% Dy + 95% Gd were also grown to assess the importance of cross-relaxation in the Sm and Dy samples. The crystals are isostructural, with monoclinic space group $P2_1/c$ and four formula units per unit cell. The first coordination sphere of Ln^{3+} consists of six Cl^- anions forming a slightly distorted octahedral $LnCl_6^{3-}$ center. The second coordination sphere is composed of nine BMI^+ cations. The emission spectra and luminescence lifetimes of both $(BMI)_3LnCl_6$ crystals and $LnCl_3$ in BMICl solution were measured. The spectroscopic similarities suggest that crystalline $(BMI)_3LnCl_6$ provides a good model of the Ln^{3+} coordination environment in BMICl solution.

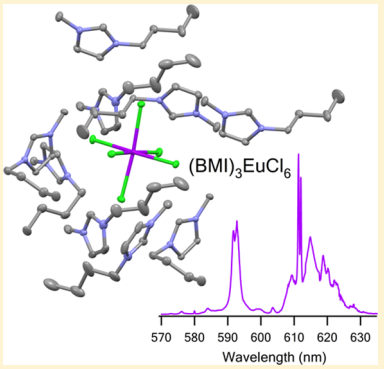

1. INTRODUCTION

Ionic liquids (ILs) are often referred to as "designer solvents", because their chemical and physical properties can be tuned by selective combination of a wide range of cations and anions.[1] ILs have many applications in catalysis,[2−5] extraction,[6−9] and electrochemistry.[10−12] They also provide excellent matrixes for luminescent lanthanide salts and complexes.[13−15] One of their most unique qualities in this regard is the potential for provision of a simultaneously fluid and nonquenching environment. The thermal stability and low vapor pressure of ILs facilitate removal of water, which strongly quenches lanthanide luminescence.[16] In fact, there have been many reports of using ILs as solvents for studying the near-infrared (NIR) emission of Nd^{3+}, Er^{3+}, and Yb^{3+}.[14,17−21] For example, Driesen et al. observed intense NIR emission from Nd^{3+} dissolved in 1-alkyl-3-methylimidazolium ILs.[21] In addition, our group has conducted a systematic study on the luminescent properties of $Ln(Tf_2N)_3$ (Tf_2N = bis(trifluoromethanesulfonyl)amide; Ln = Eu, Tm, Dy, Sm, Pr, Nd, Er) in the IL, bmpyr Tf_2N (bmpyr = 1-*n*-butyl-1-methylpyrrolidinium), and found much longer luminescence lifetimes for Ln^{3+} in this system than in conventional solvents.[20] As a novel luminescent soft material, lanthanide ions dissolved in ILs solution will continue to draw attention in spectroscopic studies.

There are also many studies focusing on the coordination environment of lanthanides in ILs. For example, Matsumoto et al. reported the crystal structure of $(EMI)_3LaCl_6$ prepared from a solution of $LaCl_3$ in the IL, EMICl-$AlCl_3$ (EMI = 1-ethyl-3-methylimidazolium).[22] Hines et al. reported single crystals of $(EMI)_3LnCl_6$ (Ln = La, Pr, Nd, Sm, Eu, Gd) from solutions of $LnCl_3$ in the IL, 1-ethyl-3-methylimidazolium chloride, and $(BMI)_3GdCl_6$ grown from a solution of $GdCl_3$ in the IL, 1-butyl-3-methylimidazolium chloride.[23] In a theoretical contribution, Chaumont and Wipff studied the solvation of lanthanide chloride salts in the ILs, [BMI][PF_6] and EMICl-$AlCl_3$, and found significant stabilization of the hexachloro complex, $LnCl_6^{3-}$, in solution.[24,25] However, although both experimental and theoretical studies suggest the likely presence of $LnCl_6^{3-}$ species in ionic liquid solution, no experimental confirmation has been reported. We pose the question: To what extent can the $LnCl_6^{3-}$ species from crystallographic studies serve as models of the coordination environment in IL solution?

An appropriate model system for solutions of $LnCl_3$ in BMICl is particularly attractive. It has been shown, for example, that, in BMICl, very little water binds to Ln^{3+} at mole ratios of water-to-IL less than 1.[26] This is in stark contrast to ILs with weakly binding anions (e.g., Tf_2N) in which water binds essentially quantitatively with Ln^{3+} in solution.[27−29] Moreover, as discussed herein, due to the low-energy-phonon environment of the $LnCl_6^{3-}$ complex, vibrational quenching of Ln^{3+} emission is dominated by the BMI^+ cations in the second coordination sphere.

In this Article, high-quality lanthanide-ion/ionic-liquid crystals $(BMI)_3LnCl_6$ (Ln = Sm, Eu, Dy, Er, Yb) were isolated from solutions of $LnCl_3$ dissolved in the popular imidazolium-based ionic liquid BMICl. The emission spectra and

Received: January 17, 2014
Published: May 21, 2014

   dx.doi.org/10.1021/ic500101x | *Inorg. Chem.* 2014, 53, 5494−5501

Table 1. Crystallographic Data and Structure Refinement for $(BMI)_3LnCl_6$ (Ln = Sm, Eu, Dy, Er, Yb)

identification	$(BMI)_3SmCl_6$	$(BMI)_3EuCl_6$	$(BMI)_3DyCl_6$	$(BMI)_3ErCl_6$	$(BMI)_3YbCl_6$
empirical formula	$C_{24}H_{45}C_{16}SmN_6$	$C_{24}H_{45}C_{16}EuN_6$	$C_{24}H_{45}C_{16}DyN_6$	$C_{24}H_{45}C_{16}ErN_6$	$C_{24}H_{45}C_{16}YbN_6$
fw	780.71	782.32	792.86	797.62	803.40
temp, K	100(2)	100(2)	100(2)	100(2)	100(2)
wavelength, Å	0.710 73	0.710 73	0.710 73	0.710 73	0.710 73
cryst syst	monoclinic	monoclinic	monoclinic	monoclinic	monoclinic
space group	$P2_1/c$	$P2_1/c$	$P2_1/c$	$P2_1/c$	$P2_1/c$
unit cell dimensions					
a, Å	9.7430(8)	9.7340(5)	9.7013(6)	9.6836(5)	9.6715(5)
b, Å	10.4786(9)	10.4776(5)	10.4692(7)	10.4703(5)	10.4650(5)
c, Å	33.499(3)	33.4766(17)	33.394(2)	33.3360(17)	33.2768(16)
β, deg	91.594(1)	91.636(1)	91.689(1)	91.705(1)	91.767(1)
vol, Å^3	3418.7(5)	3412.9(3)	3390.2(4)	3378.4(3)	3366.4(3)
Z	4	4	4	4	4
density (calcd), g/cm^3	1.517	1.523	1.553	1.568	1.585
abs coeff, mm^{-1}	2.210	2.331	2.701	2.982	3.278
$F(000)$	1580	1584	1596	1604	1612
crystal size, mm	0.25 × 0.20 × 0.10	0.62 × 0.30 × 0.20	0.30 × 0.30 × 0.30	0.50 × 0.15 × 0.15	0.35 × 0.35 × 0.30
θ range for data collection	2.04−25.36	2.04−25.42	2.04−25.39	2.04−25.44	2.04−25.44
index ranges	$-11 \le h \le 11$	$-11 \le h \le 11$	$-11 \le h \le 11$	$-11 \le h \le 11$	$-11 \le h \le 11$
	$-12 \le k \le 12$	$-12 \le k \le 12$	$-12 \le k \le 12$	$-12 \le k \le 12$	$-12 \le k \le 12$
	$-40 \le l \le 40$	$-40 \le l \le 40$	$-40 \le l \le 40$	$-40 \le l \le 40$	$-40 \le l \le 40$
reflns collected	33 771	33 763	33 193	33 375	33 173
indep reflns [R_{int}]	6278 [0.0401]	6303 [0.0225]	6246 [0.0237]	6255 [0.0208]	6233 [0.0228]
obs reflns	5512	6071	6170	5992	5937
max and min transm	0.8092 and 0.6080	0.6528 and 0.3259	0.4980 and 0.4980	0.6632 and 0.3171	0.4396 and 0.3933
data/restraints/params	6278/0/364	6303/0/364	6246/12/364	6255/12/364	6233/37/350
GOF on F^2	1.042	1.117	1.034	1.069	1.191
final R indices [$I > 2\sigma(I)$]	R_1 = 0.0240, wR_2 = 0.0488	R_1 = 0.0192, wR_2 = 0.0444	R_1 = 0.0225, wR_2 = 0.0543	R_1 = 0.0184, wR_2 = 0.0416	R_1 = 0.0256, wR_2 = 0.0538
R indices (all data)	R_1 = 0.0306, wR_2 = 0.0510	R_1 = 0.0202, wR_2 = 0.0449	R_1 = 0.0230, wR_2 = 0.0545	R_1 = 0.0195, wR_2 = 0.0420	R_1 = 0.0271, wR_2 = 0.0543
largest diff peak and hole, e Å^{-3}	0.447 and −0.531	0.472 and −0.782	0.535 and −0.895	0.711 and −0.640	1.317 and −1.047

luminescence lifetimes of the lanthanides in the crystalline matrix were compared to those in solution. We conclude that the coordination environments are remarkably similar in the two matrixes, in terms of both inner-sphere Cl^- coordination and outer-sphere BMI^+ coordination. The lanthanide-ion/ionic-liquid crystals will serve as valuable models to study the coordination environment of Ln^{3+} in BMICl solution, to test the accuracy of theoretical models describing the solvation environment, and to relate the coordination environment to the multiphonon relaxation behavior that is critical to applications as NIR phosphors.

2. EXPERIMENTAL SECTION

2.1. Materials. Samarium(III) chloride hexahydrate and erbium(III) chloride (anhydrous, 99%) were purchased from Sigma-Aldrich. Europium(III) chloride (anhydrous, 99.9%) was purchased from Acros Organics. Gadolinium(III) chloride hexahydrate (99.9%) and dysprosium(III) chloride hexahydrate (99.9%) were purchased from Alfa Aesar. Ytterbium(III) chloride (anhydrous, 99.9%) was purchased from Strem Chemicals. 1-Methylimidazole (99%), *n*-chlorobutane (CHROMASOLV, for HPLC, ≥99.8%), and activated carbon (decolorizing) were purchased from Sigma-Aldrich. Methanol (0.2 μm filtered) was purchased from Fisher Scientific. Acetonitrile (distilled in glass) was purchased from Mallinckrodt. Dimethyl sulfoxide-d_6 (D, 99.9%) was produced by Cambridge Isotope Laboratories, Inc.

2.2. Synthesis of 1-Butyl-3-methylimidazolium Chloride (BMICl). The ionic liquid BMICl was synthesized according to a literature procedure.[30] Typically, 50 mL of 1-methylimidazole was dried by adding 0.6 g of KOH and then distilled under reduced pressure. Next, in a 500 mL three-necked round-bottom flask equipped with a reflux condenser, 66 mL of *n*-chlorobutane was combined with 47 mL of the freshly distilled 1-methylimidazole. The mixture was stirred at 343 K for 7 days. After being cooled to room temperature, a yellowish solid was formed. Twenty milliliters of diethyl ether was used to wash this solid. After that, 200 mL of distilled water was added to dissolve the solid. The mixture was heated to 343 K with 4 g of decolorizing charcoal for 24 h, and then cooled to room temperature, filtered, and distilled at reduced pressure to remove water. Because at this point the product retained a slight yellow color, decolorizing charcoal was further employed multiple times until the remaining solution turned completely colorless. For these additional decolorizing steps, 300 mL of methanol and 4 g of decolorizing charcoal were added to the product. The mixture was heated at 313 K for 24 h, and allowed to cool to room temperature, filtered, and distilled at reduced pressure to remove water and methanol. The synthesized BMICl was immediately transferred into an inert-atmosphere glovebox to protect it from contamination with water.

2.3. Crystal Growth of Lanthanide-Ion/Ionic-Liquid Crystals $(BMI)_3LnCl_6$ (Ln = Sm, Eu, Gd + Sm, Gd + Dy, Dy, Er, Yb). Lanthanide-ion/ionic-liquid crystals $(BMI)_3LnCl_6$ (Ln = Sm, Eu, Gd + Sm, Gd + Dy, Dy, Er, Yb) were grown by a vapor diffusion method using acetonitrile as the antisolvent. Specifically, 10 mol % of $LnCl_3$ or $LnCl_3{\cdot}6H_2O$ was dissolved into 0.25 g of BMICl at 408 K under stirring in a glovebox to facilitate removal of water. For the Sm and Dy samples diluted in Gd, 0.5 mol % of $SmCl_3{\cdot}6H_2O$ or 0.5 mol % of $DyCl_3{\cdot}6H_2O$ was mixed with 9.5 mol % of $GdCl_3{\cdot}6H_2O$ in 0.25 g of BMICl. In each case, the mixture was then transferred to a 5 mL vial. The vial was carefully placed inside another 20 mL vial, which

dx.doi.org/10.1021/ic500101x | Inorg. Chem. 2014, 53, 5494−5501

contained 3−4 mL of CH_3CN. The larger vial was sealed and stored in the refrigerator at 277 K for ∼2 weeks without any disturbance, leading to the formation of a number of block-shaped, translucent, lanthanide-ion/ionic-liquid crystals $(BMI)_3LnCl_6$ on the bottom of the 5 mL vial, which was inside of the larger vial.

2.4. Preparation of $LnCl_3$ (Sm, Eu, Dy, Er, Yb) in BMICl Solution. Vycor ampules were made from 9 mm OD tubing with one end sealed using a hydrogen−oxygen torch. The ampules were put into the prechamber of the glovebox to remove any moisture, and then were transferred into the glovebox under argon. Within the glovebox, the $LnCl_3·6H_2O$ (Ln = Sm, Dy) or $LnCl_3$ (Ln = Eu, Er, Yb) was dissolved in BMICl at 408 K with stirring. The mixture was transferred into the Vycor ampule. The Vycor ampule was then connected to a vacuum hose with a two-way valve to protect the solution from atmosphere upon removal from the glovebox. The sample in the Vycor ampule was dried at 423 K in a temperature-controlled tube furnace for 24 h under vacuum (60 mTorr) prior to luminescence measurements. All solution concentrations are reported in units of mol % $LnCl_3$ in BMICl solution.

2.5. Characterization. The ^1H NMR spectrum of the prepared BMICl was recorded on a Varian 200 MHz spectrometer. Deuterated dimethyl sulfoxide-d_6 (DMSO-d_6) was used as a solvent to obtain the spectrum (see the Supporting Information).

Crystallographic data were collected on a Bruker APEXII at 100 K using Mo K_α radiation. Cell constants were determined after integration from more than 9000 reflections.[31] Structures were solved by direct methods using SIR97[32] and refined using SHELXL-97.[33] Data reduction and refinement were completed using the WinGX suite of crystallographic software.[34] All non-hydrogen atoms were refined with anisotropic displacement parameters, and all hydrogen atoms were placed in ideal positions and refined as riding atoms with relative isotropic displacement parameters. Molecular graphics were prepared using Mercury visualization software.[35]

The visible emission spectra and lifetime measurements for the $(BMI)_3LnCl_6$ (Ln = Sm, Eu, Gd + Sm, Gd + Dy, Dy) crystals and $LnCl_3$ in BMICl solution (Ln = Sm, Eu, Dy) were acquired using a 0.46 m flat-field monochromator (Jobin-Yvon HR460), and a time-resolved photon-counting detection system consisting of a fast, red-sensitive, side-window photomultiplier (R2949). Near infrared emission spectra and lifetime measurements for $(BMI)_3LnCl_6$ (Ln = Sm, Gd + Dy, Er, Yb) crystals and $LnCl_3$ in BMICl solution (Ln = Sm, Dy, Er, Yb) were acquired using a NIR-PMT (Hamamatsu, H10330-75) mounted on the lateral port of a 1/3 m flat-field monochromator (JY Horiba, TRIAX 320). The signal from both PMTs was preamplified (Stanford Research Systems, SR 445A preamplifier) and then fed to a multichannel scalar (Stanford Research Systems, SR 430) for time-resolved photon counting. The pulsed excitation source for lifetime measurements was provided by either a nitrogen laser/dye laser system (Laser Photonics, models UV-14 and DL-14, respectively) or by an optical parametric oscillator (Opotek, Opolette). For emission spectra, the excitation source was provided by the pulsed lasers mentioned above, or by a 5 mW 532 nm continuous wave laser for $ErCl_3$ in BMICl solution and $(BMI)_3ErCl_6$ and $(BMI)_3EuCl_6$ crystals, or by a 100 mW 940 nm continuous wave laser (Thorlabs) for $YbCl_3$ in BMICl solution and $(BMI)_3YbCl_6$ crystals.

The detection system was calibrated for relative wavelength response using a standard tungsten lamp with extended calibration out to 1700 nm (Stellar Net, SL1-CAL). All spectra were corrected for instrument response in terms of relative photon flux per wavelength interval. During the spectroscopic measurements, all $(BMI)_3LnCl_6$ (Ln = Sm, Eu, Gd + Sm, Gd + Dy, Dy, Er, Yb) crystals were kept at 278 K to prevent melting or dissolution. The solutions of $LnCl_3$ in BMICl (Ln = Sm, Dy, Er, Yb) were measured at 338 K to maintain fluidity. Solutions of $EuCl_3$ in BMICl were measured over a range of temperatures from 338 to 278 K and in a frozen glass at 77 K. During this latter measurement at 77 K, the sample, previously sealed under vacuum in a Vycor ampule, was slowly lowered into an optical quartz dewar, which was half-filled with liquid nitrogen, until the tip of the ampule was in contact with the nitrogen.

3. RESULTS AND DISCUSSION

3.1. Structural Analysis. Crystallographic data for $(BMI)_3LnCl_6$ (Ln = Sm, Eu, Dy, Er, Yb) are given in Table 1. All of the $(BMI)_3LnCl_6$ crystals are isostructural with the published crystal structure for $(BMI)_3GdCl_6$,[23] crystallizing in the monoclinic space group $P2_1/c$ with four formula units per unit cell. The crystal structure, taking $(BMI)_3EuCl_6$ as an example, is shown in Figures 1 and 2. Figure 1a illustrates the asymmetric unit, composed of three crystallographically

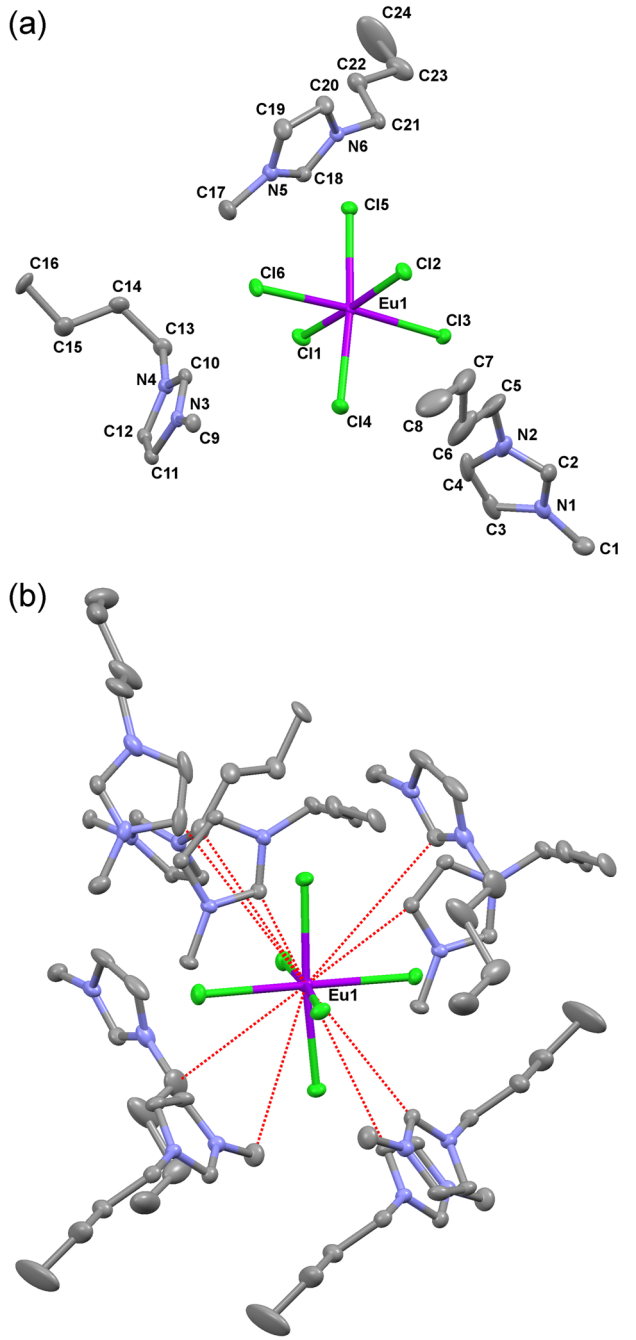

Figure 1. Molecular structure of the asymmetric unit of $(BMI)_3EuCl_6$ showing the numbering scheme in panel (a). In panel (b), the dashed lines show the distance between the Eu^{3+} ion and nearest carbon atom in each of the nine surrounding BMI^+ cations. Atoms are drawn as thermal ellipsoids with 50% probability. H atoms are omitted for clarity.

dx.doi.org/10.1021/ic500101x | Inorg. Chem. 2014, 53, 5494−5501

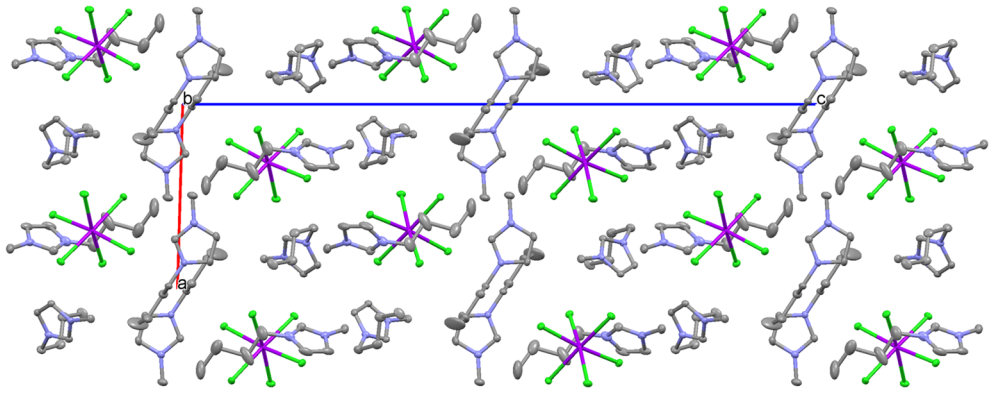

Figure 2. Crystal packing of $(BMI)_3EuCl_6$ viewed along the *b* axis. Hydrogen atoms are omitted for clarity. Other atoms are drawn as thermal ellipsoids with 50% probability. Magenta, green, blue, and gray ellipsoids represent Eu, Cl, N, and C, respectively.

Table 2. Degree of Distortion of the $LnCl_6^{3-}$ Moieties from O_h Symmetry

Ln	Sm	Eu	Dy	Er	Yb
$S(O_h)$	0.236	0.226	0.209	0.201	0.188
Ln−Cl dist (Å)[a]	2.70 ± 0.02	2.69 ± 0.03	2.65 ± 0.03	2.63 ± 0.02	2.61 ± 0.02
Cl−Ln−Cl angle (deg)[a]	90.1 ± 6.0	90.1 ± 5.9	90.1 ± 5.6	90.1 ± 5.5	90.0 ± 5.3

[a]Average bond distances and angles are given with error bars representing 2σ, twice the sample standard deviation.

independent BMI^+ cations and one unique $LnCl_6^{3-}$ anion as the metal center, consistent with the (3+) oxidation state of the lanthanide complex. The Eu−Cl bond distances range from 2.6691(5) to 2.7058(5) Å, with an average distance of 2.69 ± 0.03 Å, where the error represents 2σ, twice the sample standard deviation. The Cl−Eu−Cl angles (neighboring Cl anions) range from 85.91(2)° to 96.14(2)°, with an average angle of 90.1 ± 5.9°. Thus, the $EuCl_6^{3-}$ anion exhibits a distorted octahedral geometry. A distorted octahedral center is also found in the other $(BMI)_3LnCl_6$ crystals (Ln = Sm, Dy, Er, Yb). The degree of distortion is very similar for the five different metals, as shown in Table 2, but decreases slightly across the series. The degree of distortion of the coordination polyhedron around the lanthanide atoms was estimated by the Continuous Symmetry Measure (CSM) method.[36,37] The symmetry measure, $S(O_h)$, is a function of the minimal displacement that the atoms must undergo to achieve perfect O_h symmetry, such that $S(O_h) = 0$ for perfect octahedral symmetry and increases as the structure departs from O_h symmetry. As can also be seen in Table 2, the order of the average distance for Ln−Cl is Sm−Cl > Eu−Cl > Dy−Cl > Er−Cl > Yb−Cl, following the trend of lanthanide contraction.

The second coordination sphere of Ln^{3+} consists of nine BMI^+ cations, as shown in Figure 1b. These cations, with high-energy internal stretching vibrations, located within ~5 Å of the metal center, are important to the multiphonon quenching of Ln^{3+} luminescence. The distances between the Eu^{3+} ions and the closest carbon atom in each of nine surrounding BMI^+ cations range from 4.575 Å (Eu1−C10) to 5.687 Å (Eu1−C20), with an average of 4.942 Å. We measured similar metal−carbon distances for the other $(BMI)_3LnCl_6$ (Ln = Sm, Dy, Er, Yb) crystals and listed them in the Supporting Information. It is clear that the order of the average distances between the Ln^{3+} center and the closest C in each of nine surrounding BMI^+ cations also follows the trend of the lanthanide contraction. The largest Ln−C average distance is found in $(BMI)_3SmCl_6$ crystal at 4.948 Å, and the smallest is found in $(BMI)_3YbCl_6$ crystal at 4.911 Å. The hydrogen bonds were analyzed by the PLATON program, and details are given in the Supporting Information.

Some disorder is observed in the butyl chain of the BMI^+ cations in the $(BMI)_3LnCl_6$ crystals. Taking the structure of $(BMI)_3EuCl_6$ as an example, two sets of carbons in the butyl chain (C7−C8 and C14−C16) were each refined over two positions with an occupancy ratio of 0.634(7):0.366(7) and 0.552(8):0.448(8), respectively. Atoms C7−C8 and C14−C16 were refined as anisotropic, while C7′−C8′ and C14′−C16′ were refined as isotropic. Similar disorder appears in the other $(BMI)_3LnCl_6$ crystals (Ln = Sm, Dy, Er, Yb) and is described in the Supporting Information.

3.2. Spectroscopic Comparison between $LnCl_3$ in BMICl Solution and $(BMI)_3LnCl_6$ Crystals (Ln = Sm, Eu, Dy, Er, Yb).

3.2.1. Emission Spectra of $(BMI)_3LnCl_6$ Crystals versus $LnCl_3$ in BMICl Solution. The emission spectra of lanthanides provide a sensitive probe of the immediate coordination environment of the metal. The emission spectra of 0.3% $EuCl_3$ in IL BMICl solution at 338 K and of $(BMI)_3EuCl_6$ crystals at 278 K are shown in Figure 3. The two spectra are very similar, although the solution spectrum shows somewhat broader peaks than the crystal spectrum, as is typical. The asymmetry factor *R*, which is the ratio of the intensity of the hypersensitive $^5D_0 \rightarrow {}^7F_2$ transition to the magnetic-dipole dominated $^5D_0 \rightarrow {}^7F_1$ transition, is measured as 2.6 ± 0.4 for the crystal and 2.8 ± 0.4 for the solution species.

Temperature-dependent vibronic structure is clearly observed within the $^5D_0 \rightarrow {}^7F_0$ and $^5D_0 \rightarrow {}^7F_2$ emission manifolds. Figure 4 shows a comparison of the $^5D_0 \rightarrow {}^7F_0$ region for the IL solution and the $(BMI)_3EuCl_6$ crystals. The vibronic structure in solution has been previously reported and interpreted in terms of vibrations within the $EuCl_x^{3-x}$ moiety.[26] The vibronic transitions are labeled in Figure 4 according to their energy separation from the electronic origin. The assignment of these peaks as being vibronic in nature is confirmed by comparison of the 338 K emission spectrum with the 77 K emission spectrum of the solution. In the 77 K emission spectrum, the intensity of the anti-Stokes lines on the

dx.doi.org/10.1021/ic500101x | Inorg. Chem. 2014, 53, 5494−5501

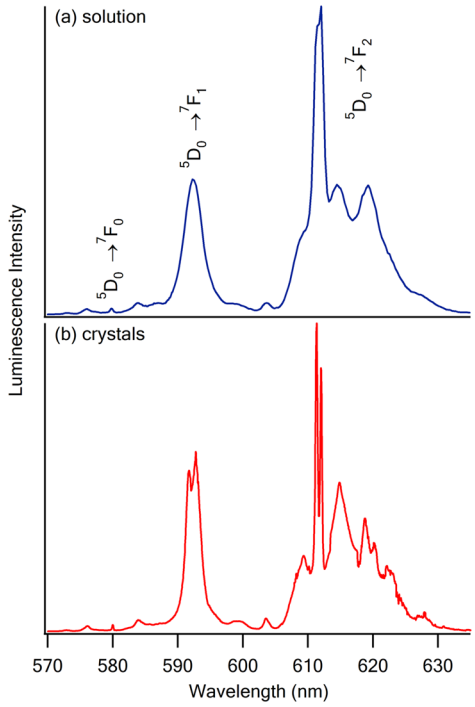

Figure 3. Emission spectra of (a) 0.3% $EuCl_3$ in BMICl solution under 526 nm pulsed laser excitation at 338 K, spectral bandwidth is 0.4 nm, and (b) $(BMI)_3EuCl_6$ crystals under 532 nm continuous wave excitation at 278 K, spectral resolution is 0.2 nm. The two spectra suggest similar coordination environments.

high-energy side of the origin is greatly reduced relative to 338 K, while the Stokes lines on the low-energy side of the origin retain their intensity. The similarities in the vibronic structure indicate very similar first coordination spheres for the solution species and crystals.

The vibronic structure around the $^5D_0 \rightarrow {}^7F_0$ electronic transition may be compared to the vibronic structure in the Eu^{3+}-doped elpasolite Cs_2NaYCl_6, where the three ungerade vibrational modes of the $EuCl_6^{3-}$ octahedral moiety are $\upsilon_3(t_{1u})$ at 235 cm^{-1}, $\upsilon_4(t_{1u})$ at 124 cm^{-1}, and $\upsilon_6(t_{2u})$ at 100 cm^{-1}, of which only the first two are coupled with the $^5D_0 \rightarrow {}^7F_0$ electronic transition.[38−41] On the basis of the energy separation, we tentatively assign the features that we observe as separated by ∼210 cm^{-1} as $^5D_0 \rightarrow {}^7F_0 + \upsilon_3$ and $^5D_0 + \upsilon_3 \rightarrow {}^7F_0$ and the features separated by ∼115 cm^{-1} from the electronic origin as $^5D_0 \rightarrow {}^7F_0 + \upsilon_4$ and $^5D_0 + \upsilon_4 \rightarrow {}^7F_0$. At 77 K in the $EuCl_3$ solution (frozen as a glass), the υ_3 mode is split (see Figure 4a), potentially by the distortion of the octahedron, although a similar splitting is observed in the elpasoslites where it is attributed to splitting of the longitudinal and transverse optical modes.[41]

Vibronic structure analogous to that shown in Figure 4 has been reported by Guillet et al. for Eu^{3+} in the RTIL 1-dodecyl-3-methylimidazolium chloride.[15] Moreover, their reported asymmetry factor (R = 2.9) and luminescent lifetime (τ = 2.81 ms) are very similar to those observed by us for $EuCl_3$ in BMICl, suggesting that Eu^{3+} in this C-12 analogue of BMICl also exhibits a distorted octahedral chloride coordination.

Figure 5 shows a comparison between the emission spectra for the $(BMI)_3LnCl_6$ crystals and those for 1% $LnCl_3$ in BMICl solution for Ln = Sm, Dy, Er, Yb. In Figure 5b, the emission spectrum of 1% $DyCl_3$ in BMICl solution is compared to that

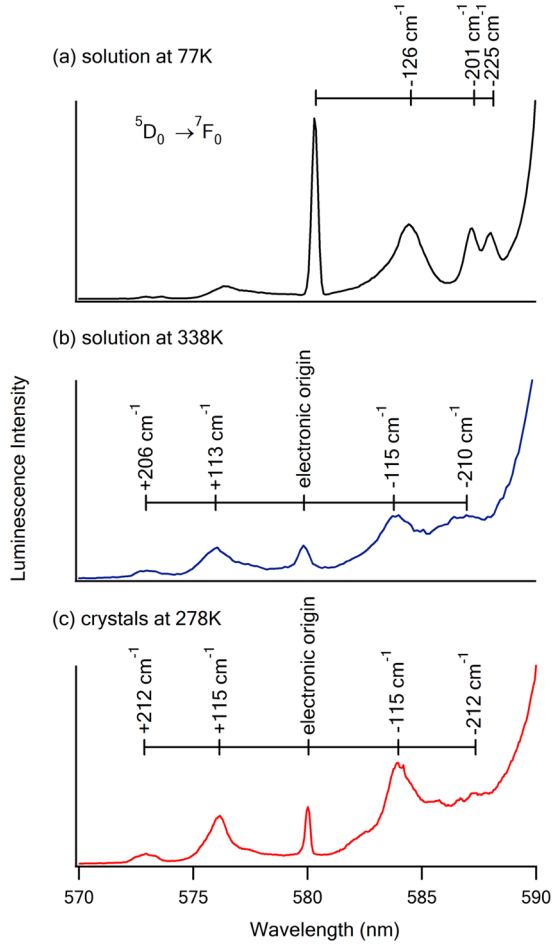

Figure 4. $^5D_0 \rightarrow {}^7F_0$ emission spectra of (a) 0.3% $EuCl_3$ in BMICl under 526 nm laser excitation at 77 K, (b) 0.3% $EuCl_3$ in BMICl under 526 nm pulse laser excitation at 338 K, and (c) $(BMI)_3EuCl_6$ crystals under 532 nm continuous wave excitation at 278 K. The vibronic transitions associated with the pure electronic $^5D_0 \rightarrow {}^7F_0$ transition are labeled according to their energy separation from the electronic origin.

of the diluted $(BMI)_3GdCl_6$:5% Dy^{3+} crystals. The spectrum from the pure crystal, $(BMI)_3DyCl_6$, is similar to that of $(BMI)_3GdCl_6$:5% Dy^{3+}. As with the Eu^{3+} analogue, the similarity in the spectra, when comparing solution to crystal, suggests that the first coordination environment is a similar $LnCl_6^{3-}$ distorted octahedron in all cases. The biggest discrepancy is observed for the Yb^{3+} solution and crystal species. The breadth of the spectral transition is typical of the crystal-field splitting of the $^2F_{7/2}$ ground state,[42,43] but the number of peaks, greater than the three expected from J = 7/2 in an octahedral field (U′ + 2E″), suggests a contribution from temperature-dependent vibronic structure.

3.2.2. Luminescence Lifetimes of $(BMI)_3LnCl_6$ versus $LnCl_3$ in BMICl Solution. The luminescence-decay rate constants, k, are sensitive to the coordination environment, most particularly to the number and proximity of potential quenching species in the first and second coordination spheres. A comparison of the luminescence-decay rate constants for the IL solutions and the corresponding crystal species is given in Table 3. All of the decay curves used to determine the k values are well fit by a single exponential function. As an example, fits to the Er^{3+} ($^4I_{13/2}$) decay curves are shown in Figure 6.

Because concentration quenching in Sm^{3+} and Dy^{3+} due to cross relaxation is commonly observed,[44,45] we prepared

dx.doi.org/10.1021/ic500101x | Inorg. Chem. 2014, 53, 5494−5501

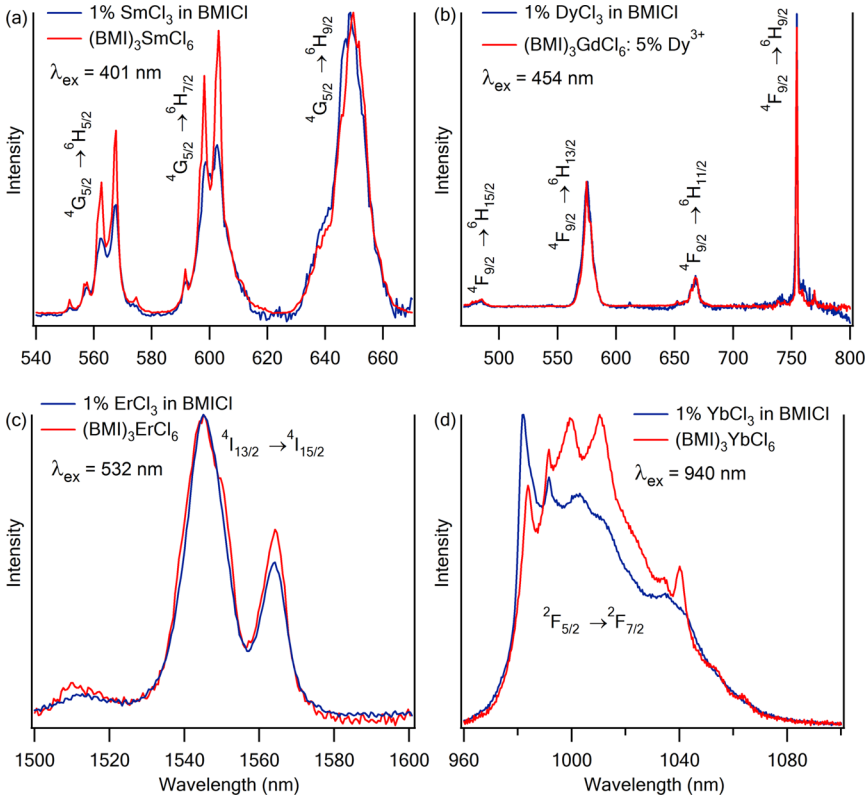

Figure 5. Normalized emission spectra of (a) 1% $SmCl_3$ in BMICl and $(BMI)_3SmCl_6$ crystals, (b) 1% $DyCl_3$ in BMICl and $(BMI)_3GdCl_6$:5% Dy^{3+} crystals, (c) 1% $ErCl_3$ in BMICl and $(BMI)_3ErCl_6$ crystals, and (d) 1% $YbCl_3$ in BMICl and $(BMI)_3YbCl_6$ crystals. Solution spectra were measured at 338 K, and crystal spectra were measured at 278 K.

Table 3. Summary of the Decay Rate Constants, *k*, for Relaxation from Emitting Levels of Several Lanthanide Ions in BMICl Solution and $(BMI)_3LnCl_6$ Crystals (Ln = Sm, Eu, Dy, Er, Yb)[a]

Ln^{3+} ($^{2S+1}L_J$)	λ_{em} (nm)	k (s^{-1}) $LnCl_3$ in BMICl solution[b]	k (s^{-1}) $(BMI)_3LnCl_6$ at 278 K	k (s^{-1}) $(BMI)_3GdCl_6$:5% Ln^{3+} at 278 K	τ_{avg} (μs)
Sm^{3+} ($^4G_{5/2}$)	648	17 860 ± 50	18 840 ± 50	18 740 ± 60	54 ± 2
Eu^{3+} ($^5D_0$)	612	331 ± 1[b]	338 ± 0		2990 ± 40
Dy^{3+} ($^4F_{9/2}$)	575	17 980 ± 40	21 130 ± 30	16 640 ± 40	58 ± 3[c]
Er^{3+} ($^4I_{13/2}$)	1545	393 000 ± 2000	393 000 ± 3000		2.5 ± 0
Yb^{3+} ($^2F_{5/2}$)	980	50 000 ± 100	51 600 ± 200		19.7 ± 0.4

[a]The last column gives the average lifetime, τ_{avg}, for the solution and crystal phases. [b]Solutions were measured at 338 K with the exception of the Eu^{3+} decay rate constant, which was obtained at 278 K. For Eu^{3+}, k exhibited a temperature dependence in solution, whereas the other lanthanide ions exhibited no observable temperature dependence. The Dy^{3+} decay rate constant was measured at 0.35 mol % to reduce the effect of concentration quenching; all other solutions are at 1 mol %. [c]For Dy^{3+}, τ_{avg} is calculated for the dilute solution and diluted crystal.

crystals with 5% Sm^{3+} or Dy^{3+} diluted in $(BMI)_3GdCl_6$. As can be seen in Table 3, the Sm^{3+} system shows essentially the same rate constant for relaxation in pure and dilute forms, whereas Dy^{3+} shows a decrease in the rate constant upon dilution, suggesting that Dy−Dy cross relaxation is a contributor to quenching in the pure crystal.

After eliminating Dy−Dy cross relaxation by means of dilution, the rate constants for the Ln^{3+} ions in IL solution and in the crystal species are remarkably similar. For Eu^{3+} ($^5D_0$), the magnitude of k is typical of radiative relaxation, suggesting little contribution from vibrational quenching. This is not surprising, given the large energy gap below the Eu^{3+} ($^5D_0$) level. However, the much faster relaxation rates observed for the other Ln^{3+} are characteristic of significant vibrational quenching. None of the measured transitions originate from excited states that are expected to be appreciably quenched by low-energy Ln−Cl stretching vibrations.[46] It seems likely, therefore, that multiphonon relaxation in these systems is dominated by the BMI^+ cations in the second coordination sphere. The similarities in the decay rate constants for the crystal and the solution species, along with the assumption that the quenching is due to second coordination sphere vibrations, suggest that even the second coordination sphere in solution is similar in structure to the crystal.

It is interesting to note that the second-coordination-sphere quenching in these systems is relatively efficient. For example, for small energy-gap lanthanides, multiphonon relaxation for $LnCl_3$ in BMICl is much more effective than that for $Ln(Tf_2N)_3$ in bmpyr Tf_2N,[20] even though the phonon cutoff for the $LnCl_6^{3-}$ complex is ∼260 cm^{-1}, whereas the maximum vibrational energy within the $[Ln(Tf_2N)_x]^{3-x}$ complex is ∼1340 cm^{-1}. As a dramatic example, the luminescence lifetime of the NIR emission from Er^{3+} ($^4I_{13/2}$) is 77 μs in bmpyr Tf_2N as compared to only 2.5 μs in BMICl.[20] Clearly, the relatively small radius of the first coordination sphere of the $LnCl_6^{3-}$

dx.doi.org/10.1021/ic500101x | Inorg. Chem. 2014, 53, 5494−5501

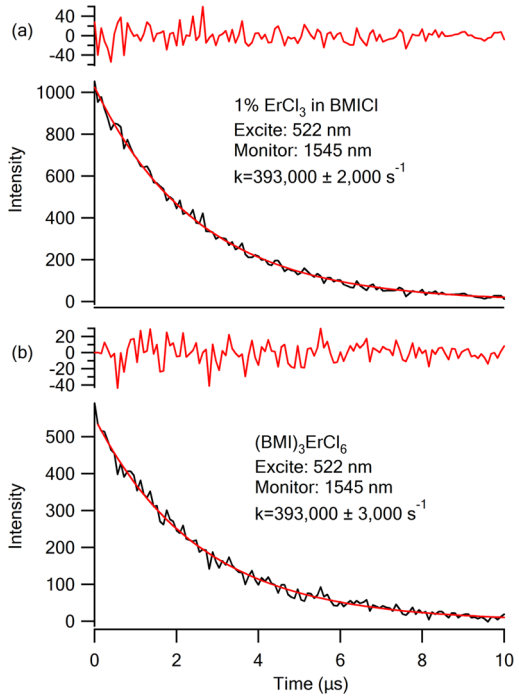

Figure 6. Luminescence decay curve for Er^{3+} ($^4I_{13/2}$) in (a) 1% $ErCl_3$ in BMICl solution and (b) $(BMI)_3ErCl_6$ crystals. The essentially identical decay rate constants suggest similar quenching environments in the two matrixes. Residuals to the single exponential fits are shown above the decay curve plots.

complex in the BMICl system provides inadequate protection from the high-energy C−H oscillators of the BMI^+ cations.

We note that, unlike the other lanthanide species investigated, the luminescence-decay rate constant for $EuCl_3$ in BMICl solution shows a temperature dependence, as illustrated in Figure 7. While the crystal and solution showed similar decay rate constants at 278 K, the rate constant for the solution increased as the temperature was raised. The temperature dependence for the crystal was not measured because the crystals had been observed to melt even at slightly elevated temperatures. The source of the temperature-dependent quenching in the solution has not been investigated by us to

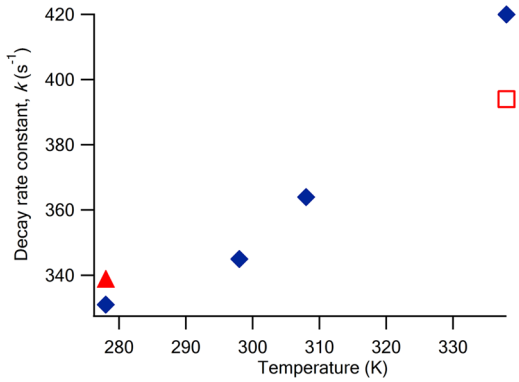

Figure 7. Decay rate constant of Eu^{3+}($^5D_0$), k, as a function of temperature for Eu^{3+}. Blue ◆ represent 1% $EuCl_3$ in BMICl solution. The red ▲ represents the $(BMI)_3EuCl_6$ crystal. The red □ represents a measurement for $EuCl_3$ in BMICl solution at 338 K from ref 26. The temperature dependence in k is not observed for other Ln^{3+} (Ln = Sm, Dy, Er, Yb).

any extent, because this observation is somewhat tangential to the purpose of the current study, which establishes that the rate constants for the crystal and solution are nearly identical if compared at the same temperature, 278 K.

However, there is some value in speculating with regard to the cause of this temperature-dependent quenching of Eu^{3+} ($^5D_0$). It is clear that it does not arise from water contamination as the study in ref 26 has shown that water does not impact the Eu^{3+} ($^5D_0$) decay rate until it exceeds 1:1 molar ratio with the BMICl solvent. In fact, multiphonon quenching of Eu^{3+} ($^5D_0$) is generally not temperature dependent in this temperature range because the relevant vibrational quanta are too large to show significant changes in the thermal populations which impact multiphonon relaxation.[47] This kind of temperature dependence is characteristic of ligand-to-metal charge transfer (LMCT) quenching in europium complexes.[48,49] Eu^{3+} is particularly susceptible to LMCT quenching, primarily due to the relative stability of Eu^{2+}. Moreover, the generally long lifetimes of Eu^{3+} ($^5D_0$) make even relatively weak quenching mechanisms observable, so that temperature-dependent changes on the order of 100 s^{-1} are quite noticeable. A reasonable candidate in our particular case is quenching through the Cl-to-Eu charge transfer state. Piguet et al. identify a Cl-to-Eu LMCT band at 33 000 cm^{-1} for polychloro-europium species in RTIL; the energy of this LMCT band falls between the high-energy threshold required for sensitization of emission and the low-energy threshold for efficient LMCT quenching.[50]

4. CONCLUSION

In this Article, a series of isostructural crystals $(BMI)_3LnCl_6$ (Ln = Sm, Eu, Dy, Er, Yb) is presented. In these crystals, Ln^{3+} ions show a distorted octahedral coordination with six Cl^- ions in the first coordination sphere and nine BMI^+ cations in the second coordination sphere. Comparison of the emission spectra of $LnCl_3$ in BMICl solution with $(BMI)_3LnCl_6$ crystals suggests that the first coordination sphere of Ln^{3+} is a similar distorted octahedron in solution. Luminescent lifetime measurements show similar decay rate constants in solution and crystals, suggesting there is also a similar second coordination sphere of Ln^{3+} in both matrixes. Future studies will focus on the contribution of second-sphere C−H oscillators to multiphonon relaxation.

■ ASSOCIATED CONTENT

Supporting Information

X-ray crystallographic data in CIF format, ^1H NMR spectrum of BMICl, molecular structure of the asymmetric unit, distances between metal and carbon atom, hydrogen-bonding geometry, and the disorder of $(BMI)_3LnCl_6$ (Ln = Sm, Dy, Er, Yb), NIR emission spectra of $SmCl_3$ in BMICl and $(BMI)_3SmCl_6$, $DyCl_3$ in BMICl and $(BMI)_3GdCl_6$: 5% Dy^{3+}. This material is available free of charge via the Internet at http://pubs.acs.org.

■ AUTHOR INFORMATION

Corresponding Author

*E-mail: smay@usd.edu.

Notes

The authors declare no competing financial interest.

dx.doi.org/10.1021/ic500101x | Inorg. Chem. 2014, 53, 5494−5501

■ ACKNOWLEDGMENTS

Support for this work was provided by the National Science Foundation (EPS-0903804) and by the State of South Dakota through the Governor's Office of Economic Development.

■ REFERENCES

(1) Binnemans, K. *Chem. Rev.* **2007**, *107*, 2592−2614.
(2) Mehnert, C. P.; Cook, R. A.; Dispenziere, N. C.; Afeworki, M. *J. Am. Chem. Soc.* **2002**, *124*, 12932−12933.
(3) Revell, J. D.; Ganesan, A. *Org. Lett.* **2002**, *4*, 3071−3073.
(4) Dupont, J.; de Souza, R. F.; Suarez, P. A. Z. *Chem. Rev.* **2002**, *102*, 3667−3692.
(5) Welton, T. *Chem. Rev.* **1999**, *99*, 2071−2084.
(6) Shimojo, K.; Kurahashi, K.; Naganawa, H. *Dalton Trans.* **2008**, 5083−5088.
(7) Wang, J.-H.; Cheng, D.-H.; Chen, X.-W.; Du, Z.; Fang, Z.-L. *Anal. Chem.* **2007**, *79*, 620−625.
(8) Katsuta, S.; Yoshimoto, Y.; Okai, M.; Takeda, Y.; Bessho, K. *Ind. Eng. Chem. Res.* **2011**, *50*, 12735−12740.
(9) Vander Hoogerstraete, T.; Onghena, B.; Binnemans, K. *J. Phys. Chem. Lett.* **2013**, *4*, 1659−1663.
(10) O'Mahony, A. M.; Silvester, D. S.; Aldous, L.; Hardacre, C.; Compton, R. G. *J. Chem. Eng. Data* **2008**, *53*, 2884−2891.
(11) Vasudeva Rao, P. R.; Venkatesan, K. A.; Srinivasan, T. G. *Prog. Nucl. Energy* **2008**, *50*, 449−455.
(12) Matsumiya, M.; Suda, S.; Tsunashima, K.; Sugiya, M.; Kishioka, S.-y.; Matsuura, H. *J. Electroanal. Chem.* **2008**, *622*, 129−135.
(13) Nockemann, P.; Thijs, B.; Lunstroot, K.; Parac-Vogt, T. N.; Görller-Walrand, C.; Binnemans, K.; Van Hecke, K.; Van Meervelt, L.; Nikitenko, S.; Daniels, J.; Hennig, C.; Van Deun, R. *Chem.—Eur. J.* **2009**, *15*, 1449−1461.
(14) Puntus, L. N.; Schenk, K. J.; Bünzli, J.-C. G. *Eur. J. Inorg. Chem.* **2005**, *2005*, 4739−4744.
(15) Guillet, E.; Imbert, D.; Scopelliti, R.; Bünzli, J.-C. G. *Chem. Mater.* **2004**, *16*, 4063−4070.
(16) Lunstroot, K.; Nockemann, P.; Van Hecke, K.; Van Meervelt, L.; Görller-Walrand, C.; Binnemans, K.; Driesen, K. *Inorg. Chem.* **2009**, *48*, 3018−3026.
(17) Eliseeva, S. V.; Bunzli, J. C. G. *Chem. Soc. Rev.* **2010**, *39*, 189−227.
(18) Arenz, S.; Babai, A.; Binnemans, K.; Driesen, K.; Giernoth, R.; Mudring, A. V.; Nockemann, P. *Chem. Phys. Lett.* **2005**, *402*, 75−79.
(19) Tiseanu, C.; Parvulescu, V. I.; Paun, C.; Dobroiu, S. *J. Nanosci. Nanotechnol.* **2010**, *10*, 2921−2925.
(20) Brandner, A.; Kitahara, T.; Beare, N.; Lin, C.; Berry, M. T.; May, P. S. *Inorg. Chem.* **2011**, *50*, 6509−6520.
(21) Driesen, K.; Nockemann, P.; Binnemans, K. *Chem. Phys. Lett.* **2004**, *395*, 306−310.
(22) Matsumoto, K.; Tsuda, T.; Nohira, T.; Hagiwara, R.; Ito, Y.; Tamada, O. *Acta Crystallogr., Sect. C: Cryst. Struct. Commun.* **2002**, *58*, m186−m187.
(23) Hines, C. C.; Cordes, D. B.; Griffin, S. T.; Watts, S. I.; Cocalia, V. A.; Rogers, R. D. *New J. Chem.* **2008**, *32*, 872−877.
(24) Chaumont, A.; Wipff, G. *J. Phys. Chem. B* **2004**, *108*, 3311−3319.
(25) Chaumont, A.; Wipff, G. *Inorg. Chem.* **2004**, *43*, 5891−5901.
(26) Samikkanu, S.; Mellem, K.; Berry, M.; May, P. S. *Inorg. Chem.* **2007**, *46*, 7121−7128.
(27) Billard, I.; Mekki, S.; Gaillard, C.; Hesemann, P.; Moutiers, G.; Mariet, C.; Labet, A.; Bünzli, J.-C. G. *Eur. J. Inorg. Chem.* **2004**, *2004*, 1190−1197.
(28) Babai, A.; Mudring, A.-V. *Chem. Mater.* **2005**, *17*, 6230−6238.
(29) Mudring, A.-V.; Babai, A.; Arenz, S.; Giernoth, R.; Binnemans, K.; Driesen, K.; Nockemann, P. *J. Alloys Compd.* **2006**, *418*, 204−208.
(30) Burrell, A. K.; Sesto, R. E. D.; Baker, S. N.; McCleskey, T. M.; Baker, G. A. *Green Chem.* **2007**, *9*, 449−454.
(31) *SAINT V6.1*; Bruker Analytical X-ray Systems: Madison, WI, 1999.
(32) Altomare, A.; Burla, M. C.; Camalli, M.; Cascarano, G. L.; Giacovazzo, C.; Guagliardi, A.; Moliterni, A. G. G.; Polidori, G.; Spagna, R. *J. Appl. Crystallogr.* **1999**, *32*, 115−119.
(33) Sheldrick, G. M. *SHELX97 - Programs for Crystal Structure Analysis (Release 97-2)*; I.f.A.C.d.U.: Tammanstrasse 4, D-3400 Göttingen, Germany, 1998.
(34) Farrugia, L. *J. Appl. Crystallogr.* **1999**, *32*, 837−838.
(35) Macrae, C. F.; Edgington, P. R.; McCabe, P.; Pidcock, E.; Shields, G. P.; Taylor, R.; Towler, M.; van de Streek, J. *J. Appl. Crystallogr.* **2006**, *39*, 453−457.
(36) Zabrodsky, H.; Peleg, S.; Avnir, D. *J. Am. Chem. Soc.* **1993**, *115*, 8278−8289.
(37) Alvarez, S.; Avnir, D.; Llunell, M.; Pinsky, M. *New J. Chem.* **2002**, *26*, 996−1009.
(38) Morley, J. P.; Faulkner, T. R.; Richardson, F. S. *J. Chem. Phys.* **1982**, *77*, 1710−1733.
(39) Flint, C. D.; Stewart-Darling, F. L. *Mol. Phys.* **1981**, *44*, 61−68.
(40) Tanner, P. A. *Top. Curr. Chem.* **2004**, *241*, 167−278.
(41) Schwartz, R. W. *Mol. Phys.* **1975**, *30*, 81−95.
(42) Koningstein, J. A. *Theor. Chim. Acta* **1965**, *3*, 271−277.
(43) Esmaeilzadeh, M.; Roohbakhsh, H.; Ghaedzadeh, A. *World Acad. Sci., Eng. Technol.* **2012**, *63*, 377−381.
(44) Zhang, X.; Seo, H. J. *J. Alloys Compd.* **2011**, *509*, 2007−2010.
(45) Li, Y.-C.; Chang, Y.-H.; Lin, Y.-F.; Chang, Y.-S.; Lin, Y.-J. *J. Alloys Compd.* **2007**, *439*, 367−375.
(46) Barasch, G. E.; Dieke, G. H. *J. Chem. Phys.* **1965**, *43*, 988−994.
(47) Struck, C. W.; Fonger, W. H. *J. Lumin.* **1975**, *10*, 1−30.
(48) Schwendemann, T. C.; May, P. S.; Berry, M. T.; Hou, Y.; Meyers, C. Y. *J. Phys. Chem. A* **1998**, *102*, 8690−8694.
(49) Fonger, W. H.; Struck, C. W. *J. Chem. Phys.* **1970**, *52*, 6364−6372.
(50) Bunzli, J.-C. G.; Piguet, C. *Chem. Soc. Rev.* **2005**, *34*, 1048−1077.